SAND2013-5304C

Heat Transfer and Pressure Drop Performance of the Air Bearing Heat Exchanger

Wayne L. Staats, PhD **Ned Daniel Matthew, BS** **Ethan S. Hecht, PhD**

Terry A. Johnson, MS **Jeff Koplow, PhD**

ABSTRACT

The thermal performance of air-cooled heat exchangers has a direct impact on the energy efficiency of many HVAC&R devices. The fundamental limitation of these air-cooled heat exchangers is the thermal resistance of the boundary layer at the solid-air interface. To improve the air side heat transfer, passive convective enhancement techniques are often employed, but these result in undesirable increases in pressure drop and higher susceptibility to fouling. The air bearing heat exchanger (ABHE), invented by Koplow (2010), circumvents some of the inherent physical limitations of conventional heat exchanger topologies and has subsequently demonstrated unprecedented air-side thermal performance, especially in volume-constrained applications.

The ABHE described in this study comprises a 10 cm diameter stationary baseplate and a rotating impeller separated by a ~10 micron hydrodynamic (i.e. self-sustained) air bearing. A thermal load is applied to the bottom of the baseplate and flows across the air bearing and into the rotating impeller. The impeller has fins that extend away from the baseplate and are shaped to act as centrifugal fan blades, inducing the surrounding ambient air to enter axially and exit radially. During this process the air absorbs the aforementioned thermal load originating from the baseplate. A key concept of the ABHE is that the hot fin surfaces reside in a rotating reference frame, which imposes a centrifugal body force on fluid particles in the boundary layer on the fins. This additional body force causes the boundary layer to remain very thin and results in an enhanced heat transfer coefficient.

In this work, we present numerical simulation results and experimental measurements to demonstrate the performance of two different 10-cm-diameter ABHE designs. We used ANSYS CFX to predict the flow and heat transfer characteristics at the free delivery point, and we validated these simulation results with several experiments: we (1) measured fan curves at several rotational speeds on a custom-made flow bench, and (2) measured the heat transfer coefficient at several rotational speeds at the free delivery point.

These results confirm that the ABHE is capable of levels of performance beyond the state-of-the-art; for example, one design was measured to have an air side primary convective heat transfer coefficient of 1990 W/m²-K at 4500 rpm. In addition, we observed that its pumping performance surpassed axial fans of comparable diameter (e.g. at 3750 rpm, it had a 150 Pa shut-off pressure and a 2370 L/min free delivery flow rate).

INTRODUCTION

The Air Bearing Heat Exchanger (ABHE), also known as the "Sandia Cooler," is shown in Figure 1 (see Koplow

Wayne L. Staats, Ned Daniel Matthew, Ethan S. Hecht, Terry A. Johnson, and Jeff Koplow are researchers at Sandia National Laboratories in Livermore, California.

(2010) for a thorough introduction). A thermal load enters the base of the device and passes through a thin (~10 micron) air gap into a rotating heat-sink-impeller. The rotating heat-sink-impeller, meanwhile, induces a radially outward flow of the ambient surrounding air. Heat transfer into this air flow occurs at the heat-sink-impeller blade surfaces. Since these surfaces reside in an accelerating frame, fluid particles in the boundary layer adjacent to their surfaces experience an outward centrifugal force, an effect which tends to result in thinner boundary layers compared to stationary, pressure-driven flow (e.g. experimental results of Cobb and Saunders (1956) or theoretical analysis of Schlichting (1979)). Since convective heat transfer is well approximated by conduction across the boundary layer, this thinning of the boundary layer represents an enhancement in the convective heat transfer coefficient.

The ABHE was invented to address the need for compact, high-performance air cooled heat sinks in electronics cooling applications, where the volume occupied by a heat sink is often constrained. As can be seen in Figure 1, the ABHE lies well beyond the performance frontier associated with commercially available heat sinks for cooling desktop CPUs for thermal resistance vs. volume occupied by the heat sink. The ABHE is now being considered for some HVAC&R applications.

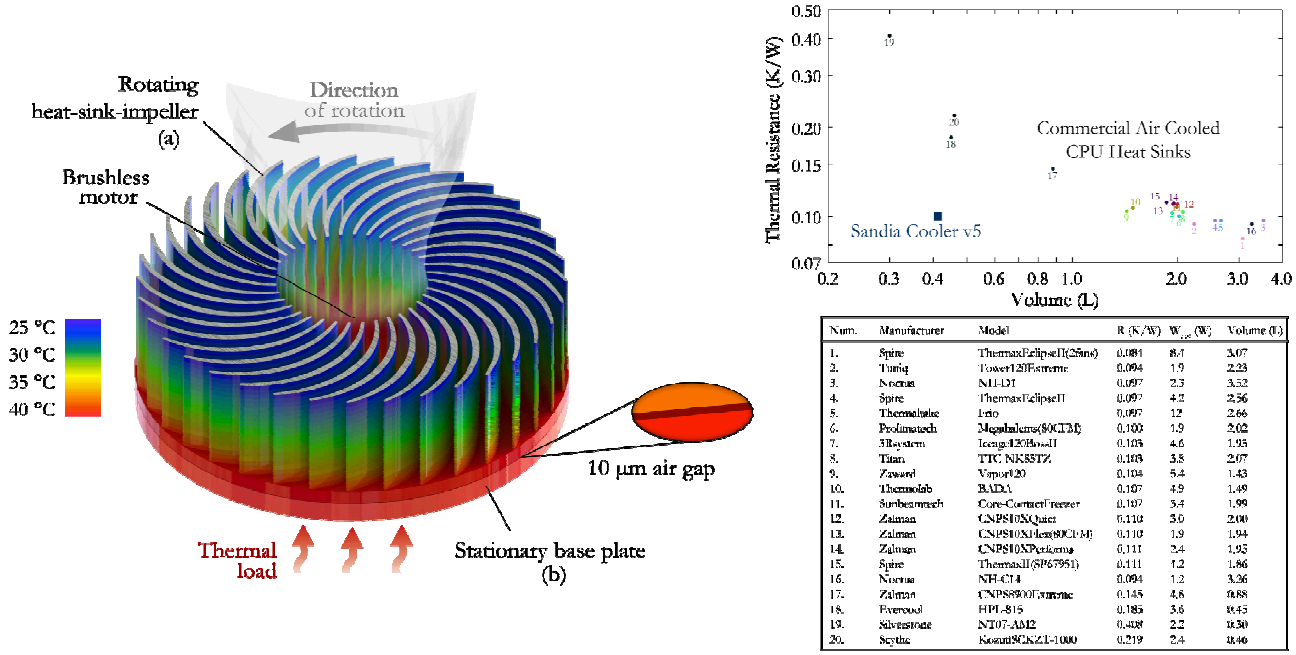

Num.	Manufacturer	Model	R (K/W)	W_{fan} (W)	Volume (L)
1.	Spire	ThermaxEclipseII(26ins)	0.081	8.7	3.07
2.	Titan	Tower120Extreme	0.094	1.9	2.23
3.	Noctua	NH-D9	0.097	2.3	3.52
4.	Spire	ThermaxEclipseII	0.097	4.2	2.56
5.	Thermaltake	Jetio	0.097	1.2	2.66
6.	Prolimatech	Megahalems(80CFM)	0.100	1.9	2.02
7.	3Rsystem	Icenga120MoonII	0.105	4.6	1.95
8.	Titan	TTC NK35TZ	0.105	3.8	2.07
9.	Zalman	Vapor920	0.104	5.4	1.43
10.	Thermolab	BADA	0.107	4.9	1.49
11.	Sunbeamtech	Core-ContactTreezer	0.107	3.4	1.99
12.	Zalman	CNPS10XQuiet	0.110	3.0	2.00
13.	Zalman	CNPS10XHeat(80CFM)	0.110	1.9	1.94
14.	Zalman	CNPS10XPerformq	0.111	2.4	1.93
15.	Spire	ThermaxII(SP67951)	0.111	1.2	1.86
16.	Noctua	NH-C14	0.094	1.2	3.26
17.	Zalman	CNPS8900Extreme	0.145	4.6	0.88
18.	Evercool	HPE-815	0.185	3.6	0.45
19.	Silverstone	NT07-AM2	0.408	2.2	0.30
20.	Scythe	KozuriSlkZ1-1000	0.219	2.4	0.46

Figure 1 *A schematic of the v4 Sandia Cooler (ABHE); the thermal load enters the bottom of the stationary base plate and flows across the thin air gap into the rotating heat-sink-impeller. The heat-sink-impeller acts as a centrifugal fan that induces an air flow that serves to absorb the thermal energy from the load. Compared to 20 commercial air cooled CPU coolers tested by Page (2012) and surveyed by Staats (2012), the Sandia Cooler has a much lower volume than heat sinks of comparable thermal resistance.*

Air cooled heat exchangers are often limited by the convection between the air and the surfaces. In heat exchangers, the overall conductance (UA) determines how much thermal interaction occurs, and thus designers often try to maximize UA to achieve better performance. However, many applications have volume constraints, which tend to limit fin surface area (A) and leaves convection enhancement as the only remaining design tool to increase UA.

A wide variety of convection enhancement techniques exist, which are discussed in the comprehensive review of Bergles (1998). These techniques consist of passive (e.g. rough surfaces, extended surfaces, swirl flow devices, etc.) and

active (e.g. stirring, surface scraping) methods. The ABHE represents a unique type of active enhancement because the enhancement mechanism (associated with the rotation of the heat-sink-impeller) is also necessary for establishing relative motion between the heat sink fins and ambient air and moving the air through the system.

In the present work, we discuss results of CFD and experiments for two prototype ABHEs, which we refer to as "v4" and "v5." We tested the pumping performance (pressure rise vs. volume flow) using a flow bench to determine the fan curves at several rotational speeds. In addition, we conducted steady-state thermal testing to measure the convective thermal resistance (average heat transfer coefficient) of the rotating impellers. Finally, we showed that the performance trends at the free delivery flow rate can be captured with a relatively simple CFD model.

EXPERIMENTS

We performed several experiments to measure the performance of the ABHE. First, we used a custom-built apparatus to measure the fan curves (pressure rise vs. volume flow) of the device at various speeds. Second, we measured the thermal performance at the free delivery point using a thin film heater and an IR thermometer.

Fan Curve Measurement

The fan testing apparatus, shown in Figure 2, allowed for the flow rate through the cooler to be restricted and the pressure just upstream of the cooler to be measured. In this apparatus, a DC motor drove the cooler, which was situated just underneath a plenum whose pressure was monitored relative to the ambient.

A series of commercial sieves were modified to make up the flow plenum from which the impeller drew air. The mesh (140 and 20 mesh) sieves served to straighten and spread the inlet flow, minimizing jetting onto the impeller. By drawing air from a large volume (305 mm diameter by 203 mm height, to the screen nearest the impeller), the flow to the impeller was made to be as natural as possible, with the constraint that the inlet and outlet of the impeller needed to be separated. The system resistance was varied using a combination of a flow booster and butterfly valve. Using a flow booster (Nortel Manufacturing AM750, or AM1000, for low and high flow rates, respectively) allowed measurements to be made all the way out to the free delivery point (and also into the negative pressure regime, although this is of little practical interest). A turbine flow meter (Omega FTB-934 or FTB-938, for low and high flow rates, respectively) was used to measure the gas flow. A differential pressure transducer (Omega PX275-05DI) was used to measure the pressure rise across the impeller. The rotation was controlled by a DC motor (Pittmann 14204S005) and a variable power supply (Circuit Specalisits 3646A) that was computer controlled. The rotational speed was characterized using a stroboscope and related to the motor voltage, which was measured throughout the course of the experiments. Finally, we performed two sensitivity checks to ensure negligible systematic errors due to (1) the position of the impeller relative to the plenum (where there is a small clearance between the top edge of the heat-sink-impeller and the plenum) and (2) the position of the total pressure tap in the plenum.

Since the cross sectional area of the plenum is much larger than the cross sectional area of the inlet to the cooler, the velocity in the plenum is small and the dynamic pressure ($\rho v^2/2$) is negligible compared to the total pressure, meaning that the static and total pressures can be considered equal in the plenum. Thus, the differential pressure measurement in the experimental apparatus represents the total-to-static pressure rise across the impeller (for a discussion of the utility of using the total-to-static pressure as a performance metric, see Epple et al. (2011)). At a given rotational speed, the total-to-static pressure rise across the impeller depends on the flow resistance of the system in which it is installed; this resistance was varied in the experimental apparatus in order to yield fan curves for various rotational speeds (i.e. total-to-static pressure rise vs. volume flow). These fan curves can be seen in Figure 3 for two impeller designs. At a speed of 2500 rpm, both impellers had a shut-off pressure of 65 Pa and a volumetric flow rate of order 1500 L/min. Near the free delivery point, the fans (most noticeably the v5 impeller) experienced a hysteresis effect, where either of two stable flow rates were possible depending on the pressure from which the operating point was approached. The fits shown in Figure 3 are based on fits to

the dimensionless fan curves (discussed below and shown in Figure 2).

The fan curves were nondimensionalized by dividing the volume flow and pressure rise by reference quantities. The flow coefficient (φ) is formed by normalizing the volume flow to a hypothetical flow rate, where the velocity is the impeller tip speed ($\omega d/2$) and the cross sectional area is the impeller's exit plane area (πdb):

$$\varphi = \frac{\dot{V}}{\pi \omega d^2 b/2}, \tag{1}$$

where $\dot{V}$ is the volume flow rate, ω is the rotational speed (rad/s), d is the outer diameter of the impeller, and b is the axial breadth (height) of the impeller at the exit plane. The total-to-static head coefficient (ψ_{ts}) is formed by normalizing the total-to-static pressure rise to the dynamic pressure associated with the impeller tip speed ($\rho v^2/2$):

$$\psi_{ts} = \frac{\Delta p_{ts}}{\rho \omega^2 d^2/4}, \tag{2}$$

where Δp_{ts} is the total-to-static pressure difference and ϱ is the fluid density. Note, however, that for mathematical convenience the denominator is multiplied by 2 (a discussion of this can be found in Epple (2011)). This definition also means that, in relation to the velocity triangle commonly analyzed in fan design, the flow and flow coefficient have consistent and direct interpretations as ratios of the meridional and tangential exit velocities to the tip speed, respectively.

By forming these dimensionless quantities, the multitude of fan curves shown in Figure 3 can be compressed into a single curve for each impeller, as shown in Figure 2. The curves in Figure 2 were used to reconstruct the fan curve at any speed or for a different size impeller (provided geometric similarity is maintained and the device is not operated in a different flow regime). The dimensionless fan curves exhibited two parabolic regions; the fits used a sigmoid function to blend these two parabolic regions. Compared to v4, v5 had a similar shut-off head coefficient and a slightly higher free delivery flow coefficient. Also, relative to v4, the kink that occurs at about 2/3 of the free delivery flow coefficient was more pronounced in v5.

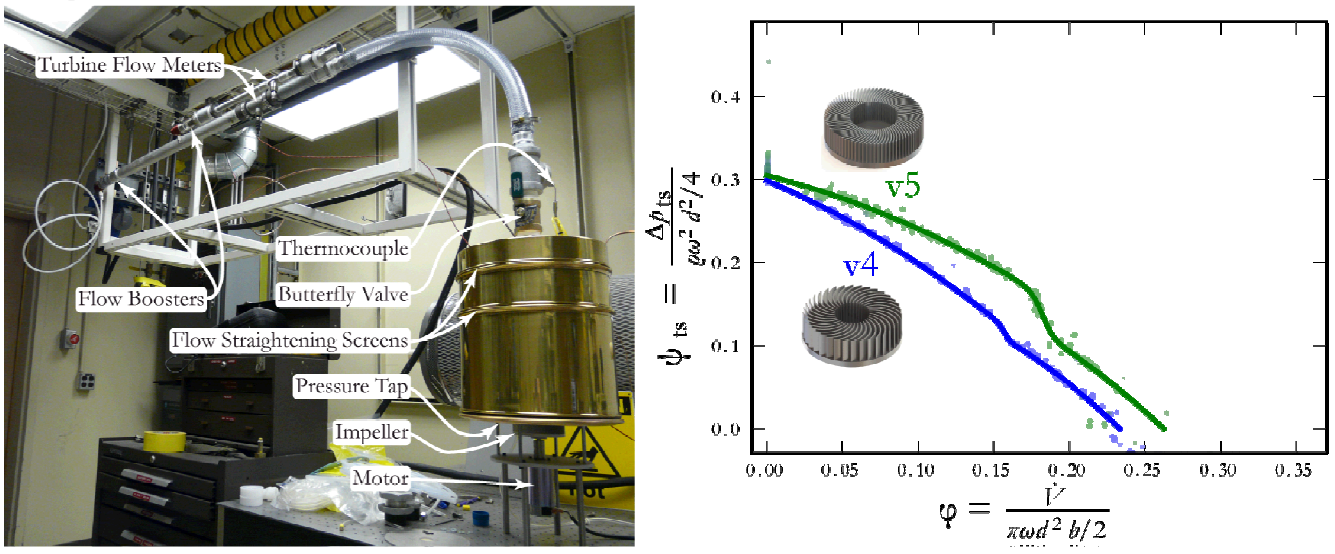

Figure 2 *The experimental apparatus used to measure the fan curves (left); the dimensionless fan curves (total-to-static head coefficient vs. flow coefficient) for the v4 and v5 impeller designs (right).*

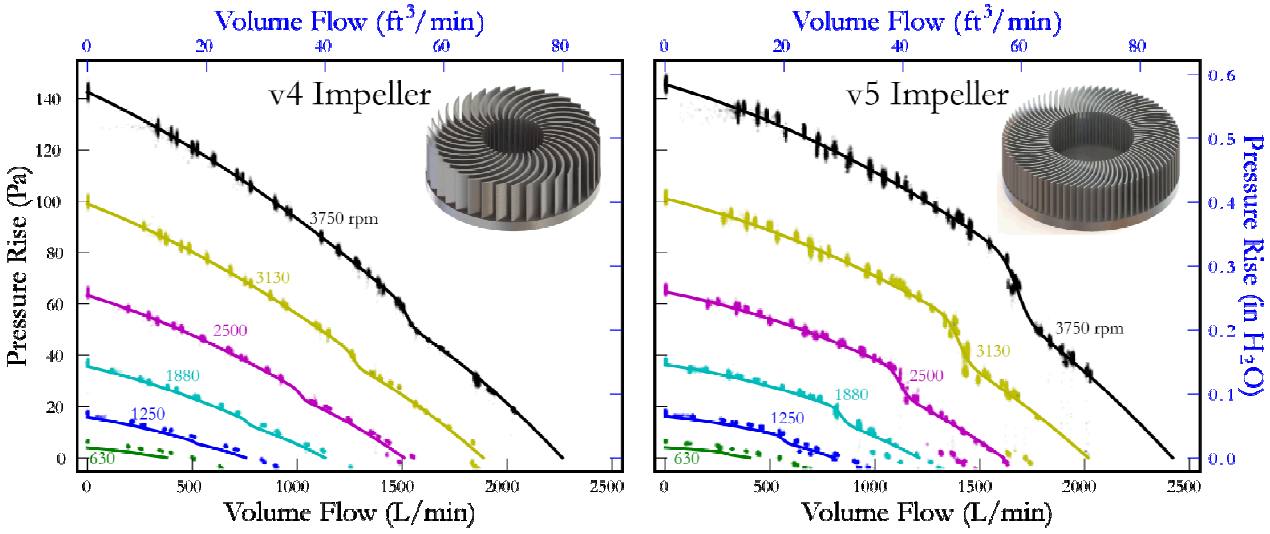

Figure 3 Fan curves for the v4 impeller (left) and v5 impeller (right).

Heat Transfer Measurement

The heat transfer performance of the v4 and v5 heat-sink-impellers was measured using the apparatus shown in Figure 4. A Kapton film heater was adhered to the bottom surface of the impeller, covered with insulation and then mounted on a rotating shaft. The contact area between the shaft and the base of the impeller was very small, which, in addition to insulation, minimized conduction through the shaft. The power leads to the heater were fed through two of the blades of the impeller, into a 305 mm long piece of 4 mm hex tubing where they were mated with a rotary electrical connector (Mercotac 205-H). Two IR thermometers sited to the impeller provided temperature readings (Fluke 80T-IR and Omega OS36-01). A type-K thermocouple measured the temperature of the inlet air. The voltage and current applied to the heater were measured as well as the rotation speed (by measuring the voltage waveform on one of the phases of the brushless DC motor). All voltages were logged with a data acquisition system (Agilent 34970A). The heater voltage measurements were corrected for a 0.2Ω resistance in the heater wiring (including the rotary electrical connector). The current was determined by measuring the voltage drop across a 0.05Ω current viewing resistor.

In these tests, the temperature of the cooler's base was measured for various thermal power inputs in the 50-100 W range. The overall convective thermal resistance (R_{conv}) was calculated as $R_{conv}=(T_{base}-T_{amb})/Q$, where Q is the heat transfer into the impeller, T_{base} is the temperature of the impeller base, and T_{amb} is the temperature of the surrounding ambient air. Notice that the temperature scale associated with R_{conv} is the *inlet temperature difference* of the heat sink. In series with the convective thermal resistance, however, is the thermal resistance of the air gap, which can be calculated using Fourier's Law as $R_{gap}=b_{gap}/kA_{base}$, where b_{gap} is the air gap breadth, k is the thermal conductivity of air, and A_{base} is the area of the impeller base. Typically, we have run these impellers with a 10 micron air gap, which yields a gap thermal resistance of 0.047 K/W (the thermal resistance per unit gap width is 4700 K/W/m). From the definition of R, an "effective" heat exchanger UA can be calculated as $UA=1/R_{total}$. Since the thermal resistance of the gap is in series with the convective thermal resistance, the overall effective heat transfer coefficient (U) can be calculated as $U=1/[(R_{conv}+R_{gap})A_{base}]$. Again, in considering U one must recall that it refers to the thermal circuit starting at the bottom of the stationary baseplate (T_{bot}) and ending at the ambient surrounding air (T_{amb}), and therefore has the temperature scale T_{bot}-T_{amb}. This is appropriate for heat sink design, where one has knowledge of these temperatures a priori and is not concerned with the temperature profile in the air flow; however, it is different than the temperature scale used in considering the flow of the air in the impeller (for

example, in an effectiveness-NTU analysis), which is the log-mean temperature difference. It is straightforward to convert to the log-mean temperature difference by performing an energy balance on the air flow.

Finally, the heat exchanger effectiveness is defined as the increase in the air's bulk temperature relative to the inlet temperature difference: $\varepsilon=(T_{out}-T_{amb})/(T_{base}-T_{amb})$. In Figure 5, the convective thermal resistance (R_{conv}), the overall effective heat transfer coefficient (U), and the air-side heat exchanger effectiveness are shown for v4 and v5 as a function of rotational speed.

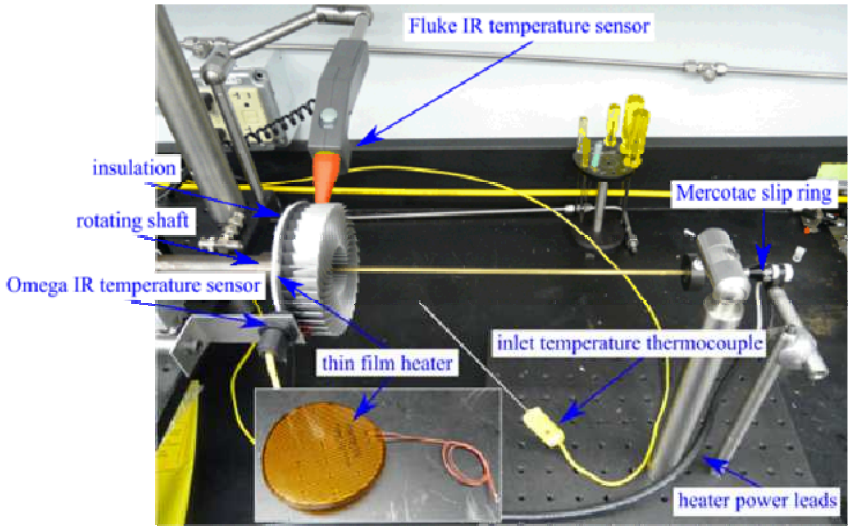

Figure 4 *The thermal performance of the heat-sink-impellers was characterized by heating the base with a Kapton film heater and measuring the resultant base temperature with two IR temperature sensors. Electrical power was delivered to the rotating thin film heater/impeller assembly via a rotary electrical contact.*

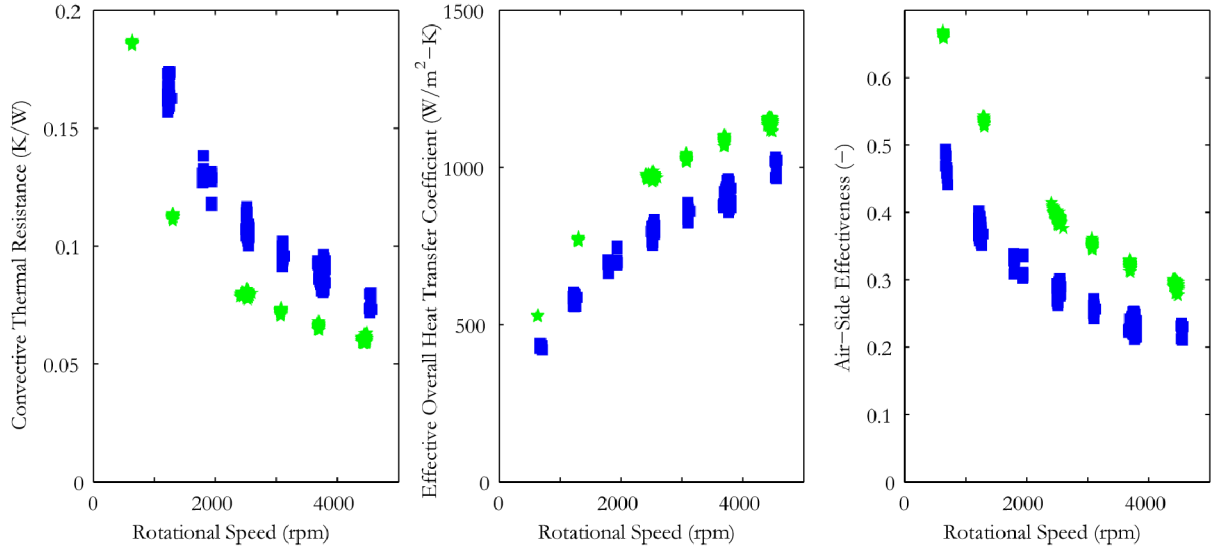

Figure 5 *(a) The convective thermal resistance of the heat-sink-impellers decreases with increasing rotational speed, and v5(green) achieves lower thermal resistance than v4 (blue). Note: the convective thermal resistance does not include the air gap thermal*

resistance. (b) Assuming a 10 micron air gap, the effective overall heat transfer coefficient was calculated, with the temperature scale being T_{bot}-T_{amb}. Adjustment of the air gap distance entails a tradeoff between lower air gap thermal resistance and higher shearing losses. For example, in the case of a 10-cm-diameter ABHE, a 10 micron air gap results in an air gap thermal resistance of 0.047 K/W and 1.8 W of mechanical power dissipation due to shearing in the air gap at 2500 rpm, whereas an air gap distance of 5 microns would result in an air gap thermal resistance of 0.024 K/W and 3.6 W of frictional loss at 2500 rpm. The optimum air gap distance is therefore application dependent. (c) The effectiveness of the single-stream heat exchanger on the air side was calculated; to obtain an estimate of T_{out} of the air flow, an energy balance on the air was performed, based on the free delivery mass flow rate as measured in the fan testing apparatus. Compared to v4, v5 exhibited a higher effectiveness at a given rotational speed.

SIMULATIONS

To better understand the fluid dynamics in the heat-sink-impeller of the ABHE, we developed a computational fluid dynamics (CFD) model using ANSYS CFX. This model consisted of a single unit cell comprising one blade of the heat-sink-impeller, as shown in Figure 6. The conjugate heat transfer capability of CFX was used to include the coupling between the solid conduction in the aluminum fins and convection heat transfer to the air flow. Stationary and rotating domains were used with a frozen rotor frame change model at the stationary-rotating interface. The edges of the unit cell were periodic interfaces. Finally, air was allowed to enter and leave the domain via the top, bottom, and side faces by using an opening boundary condition, which specifies either the static or total pressure for exiting or entering flow, respectively. The openings were situated far enough from the impeller to allow the flow field to adjust itself to become relatively uniform at the boundary.

The bottom of the impeller was given a constant temperature boundary condition (chosen to be 25 C higher than the ambient surroundings) in order to mimic the surface of a vapor chamber heat pipe, which is used in CPU cooling applications to effectively spread the concentrated thermal load over the entire air gap area. The heat transfer into the impeller was determined with an area integral of the heat flux into the constant temperature boundary. The flow was modeled using the SST turbulence model with the total energy equation. According to a study by Brethouwer (2011) of heat transfer in rotating channels, the turbulent Prandtl number is lower than the typical value of 0.9 for a stationary channel. Based on this, as well as comparisons to experimental results, the turbulent Prandtl number was set to 0.2 (rather than the default value of 0.9 in CFX).

Representative results from the CFD solutions can be seen in Figure 6, which shows several repeated unit cells of the v5 impeller. The velocity vectors are projected onto (1) a surface running down the middle of a unit cell and (2) a surface parallel to the impeller base and situated at half the blade height. These surfaces are colored by temperature, as is the exterior surface of the aluminum blades. The isotherms on the fin surfaces indicate higher heat transfer at the edge of the fin near the inner diameter, where the boundary layer begins. Also, the velocity vectors indicate that air flow enters the channel from the top as well as the inner bore. Finally, the thermal resistance results from the CFD model overpredicts the measured thermal resistance, but correctly captures the trends of v4 and v5, and predicts a lower thermal resistance for v5. The CFD predictions for volumetric flow rate and torque are typically within 15% of the experimental results.

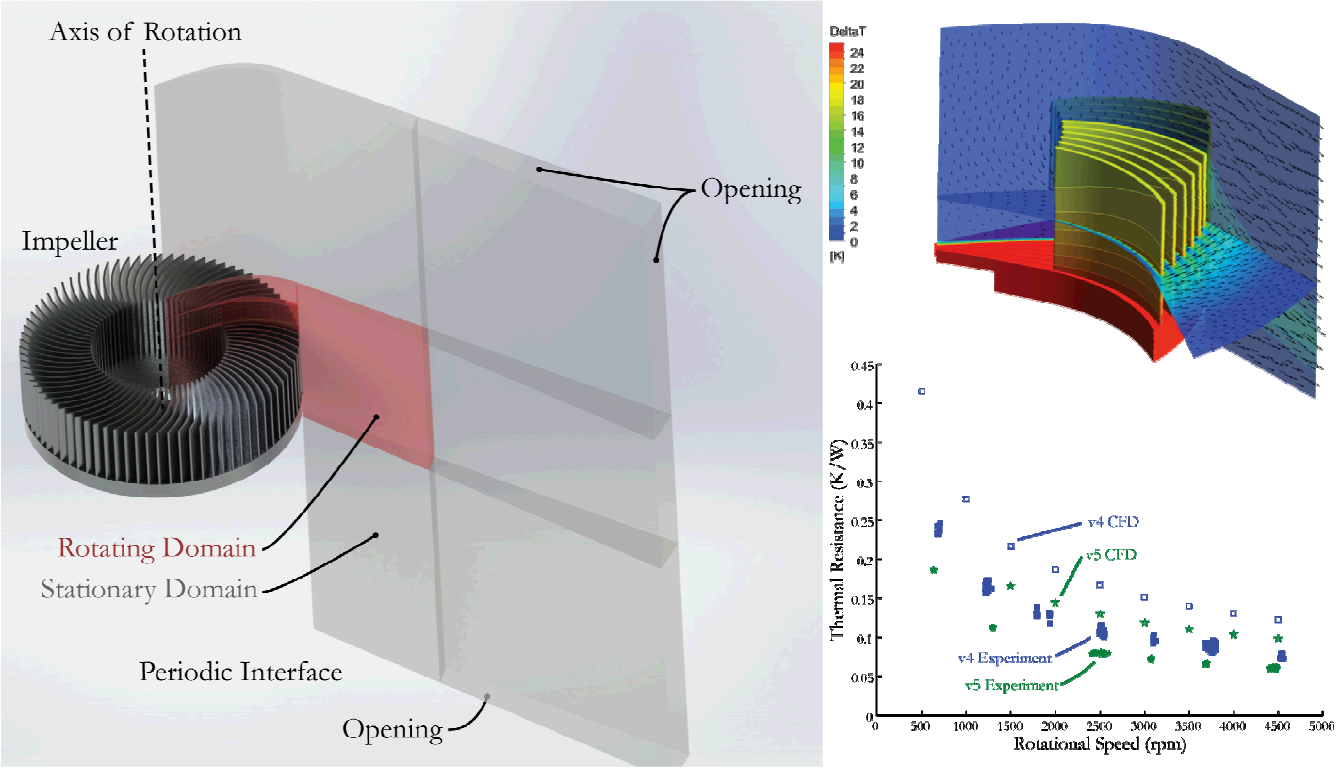

Figure 6 *The CFD simulations used a stationary (gray) and rotating (red) domain, with rotational periodicity to reduce the number of elements and the computation time. In this schematic the entire impeller is shown for clarity. The upper right diagram shows velocity vectors projected on the middle of the unit cell and velocity vectors projected on a plane parallel to the base of the impeller. Both planes and the impeller surfaces are colored by temperature relative to the ambient temperature. The CFD simulations correctly predict the trends in thermal resistance, but the values are consistently higher than the experimental data.*

CONCLUSION

The ABHE, invented for volume-constrained CPU cooling applications, has been shown to have unprecedented compactness and thermal performance. We report experimental results (fan curves and thermal resistance at the free delivery point) for two 10-cm-diameter heat-sink-impeller designs. One of the heat-sink-impellers we tested had an air side primary heat transfer coefficient of 1990 W/m^2-K at 4500 rpm; when considering a 10 micron air bearing gap in series, the effective heat transfer coefficient seen on the bottom of the stationary baseplate was 1150 W/m^2-K. In addition, we observed that its pumping performance surpassed axial fans of comparable diameter (e.g. at 3750 rpm, it had a 150 Pa shut-off pressure and a 2370 L/min free delivery flow rate). Finally, we show that a CFD model of a single-blade unit cell can yield satisfactory predictions that capture the trends in thermal resistance, yielding useful design information.

ACKNOWLEDGMENTS

Sandia National Laboratories is a multi-program laboratory managed and operated by Sandia Corporation, a wholly owned subsidiary of Lockheed Martin Corporation, for the U.S. Department of Energy's National Nuclear Security Administration under contract DE-AC04-94AL85000. The authors thank the Building Technologies Program (US Department of Energy, Office of Energy Efficiency and Renewable Energy) and the Sandia Laboratory Directed Research & Development (LDRD) program for supporting this research.

REFERENCES

ANSYS CFX, Release 14.5.

Brethouwer, G. et al., Turbulence, instabilities and passive scalars in rotating channel flow, J. Phys.: Conf. Ser. 318 032025, 2011.

Bergles, A.E., Handbook of Heat Transfer, ch. 11: Techniques to Enhance Heat Transfer. McGraw–Hill, 1998.

Cobb, E.C. and Saunders, O.A., "Heat transfer from a rotating disk," Proceedings of the Royal Society of London, Series A, Mathematical and Physical Sciences, vol. 236, no. 1206, pp. 343–351, 1956.

Epple, P., Durst, F. and Delgado, A., A theoretical derivation of the Cordier diagram for turbomachines. Proceedings of the Institution of Mechanical Engineers, Part C: Journal of Mechanical Engineering Science, 225: 354-368, doi:10.1243/09544062JMES2285, February 1, 2011.

Koplow, J.P., "A fundamentally new approach to air-cooled heat exchangers," Technical Report SAND2010-0258, Sandia National Laboratories, 2010.

Page, M., "FrostyTech – Best Heat Sinks & PC Cooling Reviews." http://www.frostytech.com. Accessed: March, 2012.

Staats, W.L., "Active heat transfer enhancement in integrated fan heat sinks," doctoral dissertation, Massachusetts Institute of Technology. http://hdl.handle.net/1721.1/78179, 2012.

Schlichting, H. "Boundary-layer theory," Seventh edition, McGraw-Hill series in mechanical engineering, pp. 102—107, 1979.